Thermal decomposition and fractal properties of sputter-deposited platinum oxide thin films

Adolfo Mosquera
Instituto de Ciencia de Materiales de Madrid, Consejo Superior de Investigaciones Científicas, E-28049 Madrid, Spain

David Horwat[b)]
Institut Jean Lamour, Ecole des Mines de Nancy, 54042 Nancy, France

Luis Vazquez
Instituto de Ciencia de Materiales de Madrid, Consejo Superior de Investigaciones Científicas, E-28049 Madrid, Spain

Alejandro Gutiérrez
Departamento de Física Aplicada and Instituto Nicolás Cabrera, Universidad Autónoma de Madrid, E-28049 Madrid, Spain

Alexei Erko
Helmholtz-Zentrum Berlin für Materialien und Energie GmbH, Elektronenspeicherring BESSY II, 12489 Berlin, Germany

André Anders[b)]
Lawrence Berkeley National Laboratory, University of California, Berkeley, California 94720

Joakim Andersson[b)]
The Angstrom Laboratory, Uppsala University, S-75121 Uppsala, Sweden

Jose L. Endrino[a),b)]
Abengoa Research, Campus Palmas Altas, E-41014 Sevilla, Spain

(Received 17 August 2011; accepted 21 October 2011)

Porous platinum thin films were prepared by thermal decomposition at temperatures from 25 to 675 °C of platinum oxide films deposited by a pulsed reactive sputtering technique. The samples' chemistry and structure were investigated by x-ray diffraction (XRD), x-ray photoelectron spectroscopy (XPS), and x-ray absorption near edge structure (XANES), showing that the decomposition of the oxide begins as low as 400 °C and follows a sigmoidal trend with increasing annealing temperature. In the XRD spectra, only an amorphous-like signature was observed for temperatures below 575 °C, while Pt 4f XPS showed that the deposited oxide was a mixture of PtO_2 and PtO. Pt-L_3 edge XANES and Pt 4f XPS spectra showed that the Pt concentration and electronic structure are predominant for temperatures equal to or above 575 °C. The morphologies of the films were investigated by the area-perimeter method from atomic force microscopy and scanning electron microscopy (SEM) images, indicating that the surfaces exhibit a combination of Euclidian and fractal characteristics. Moreover, the thermal evolution of these characteristics indicates the agglomeration of the grains in the film as observed by SEM.

I. INTRODUCTION

Porous platinum thin films are of significant technological importance because they can be used as catalysts,[1,2] electrodes,[3] and as components of fuel cells and sensors.[4,5] Porous platinum oxide films could serve as precursors to achieve high specific surface area in platinum electrodes.[6] The variety of porous platinum is recognized in three different states: platinized platinum, platinum sponge, and platinum black,[7] allowing coatings with different characteristics. For instance, platinum black is a dispersed black powder with a specific surface area of 30–40 m^2/g[8] used for the fabrication of platinized electrodes with applications in microfabricated solid state, chemical and biological sensors.[9,10] It can be obtained by electroplating smooth, clean metal foils in a chloroplatinic acid solution[7] and by physical-vapor-deposition

a)Address all correspondence to this author.
e-mail: jose.endrino@research.abengoa.com
b)This author was an editor of this focus issue during the review and decision stage. For the *JMR* policy on review and publication of manuscripts authored by editors, please refer to http://www.mrs.org/jmr-editor-manuscripts/
DOI: 10.1557/jmr.2011.418

techniques such as reactive sputtering.[11] The large surface area of porous platinum coatings can be achieved in some cases through the control of electrochemical reduction,[12] hydrogen reduction, thermal annealing,[13] and also by laser irradiation[14] of platinum oxide.

Thermal decomposition is a chemical reaction where a compound breaks up into simpler compounds or elements when heated. The thermal decomposition of amorphous platinum oxide (a-PtO_x) has been studied in different atmospheres such as nitrogen and oxygen[6,15–17] to find the different phases (α-PtO_2, PtO, Pt_3O_4, and Pt) and their relative amounts upon the decomposition process. It has recently been shown that adding Pt into PdO films lowers their decomposition temperature,[18] which can improve the catalytic combustion of methane.[19,20]

Atomic force microscopy (AFM) and scanning electron microscopy (SEM) are powerful tools for the investigation of the fractal dimension of surfaces including those of thin films.[21–23] The concept of fractal geometry introduced by Mandelbrot[24] provides a useful framework for quantifying the morphological complexity of a vast range of irregular objects, including surfaces,[25] through its fractal dimension, which is denoted by D. The surface fractal dimension D_s, with values between 2 and 3, describes quantitatively the degree of surface irregularity, where $D_s \rightarrow 3$ describes that the surface is highly irregular. As PtO_x films experience a microstructural and morphological reorganization upon annealing, the investigation of their surface fractal dimension can serve as a platform for understanding their optical, catalytic, and electronic properties.

The present work describes an experimental investigation of the decomposition of platinum oxide PtO_x thin films upon thermal annealing. Specifically, the evolution of phase composition, structural state, and surface morphology are investigated. In addition, the area-perimeter (AP) method[26] was applied to estimate the fractal dimension using AFM and SEM images of the films in the as-deposited state and after annealing at different temperatures.

II. EXPERIMENTS

Thin platinum oxide films were deposited using reactive pulsed magnetron sputtering from a 50-mm-diameter platinum target in a pure oxygen atmosphere. The magnetron was driven by a PINNACLE PLUS (Advanced Energy, Filderstadt, Germany) power supply applying average power and current of 100 W and 0.21 A, respectively, with a pulsing frequency of 325 kHz and a reverse time of 1 μs. The sputtering chamber was evacuated to a working pressure of 24 mtorr (3.2 Pa) using rotary and turbomolecular pumps. Flow controllers (MKS, MKS Flow Measurement & Control Products, Andover, MA) were used to control the flow rate of pure oxygen (25 sccm). The distance between the target and substrate holder was fixed at 11 cm. The films were deposited on Si(111) substrates. Each film sample with an as-deposited thickness of about 500 nm was annealed in air using a furnace model BLUE M 1500 (Thermal Product Solutions, New Columbia, PA) at a heating rate of 8 °C/min, with holding temperatures, 5 min each, at 25, 400, 450, 500, 550, 575, 600, 625, and 675 °C, followed by removing the sample from the furnace and letting it cool down in ambient air.

Phase identification was performed using a BRUKER D8 x-ray diffractometer with Cu Kα radiation over an angle range of $2\theta = 15–60°$ (Bruker AXS, Madison, WI). X-ray photoelectron spectroscopy (XPS) was performed with monochromatic Al radiation (1486.74 eV). Binding energies were measured with a PHOIBOS150 9MCD (SPECS Surface Nano Analysis, Berlin, Germany) hemispherical electron energy analyzer, and the compositional analysis was conducted with the CASAXPS program, using the Pt 4f core level peak.

Pt-L_3 total fluorescence yield x-ray absorption near edge structure (TFY-XANES) spectra were obtained on the KMC-2 beamline located at the HZB storage ring BESSY II, Berlin, Germany. In the TFY mode, the emitted and registered x-rays are predominantly from the bulk of the material, rather than the surface layers.

AFM characterization of the thin films annealed at different temperatures was carried out using a NANOSCOPE IIIa (Veeco, Plainview, NY) and an AGILENT 5500 (Agilent Technologies, Santa Clara, CA). The areas scanned for the images were from 1 μm × 1 μm to 30 μm × 30 μm and each image was composed of 512 × 512 pixels.

SEM images of the as-deposited films and films annealed at 25, 575, 600 and 675 °C were obtained using a NANOSEM 230 with secondary electron detection (FEI, Eindhoven, The Netherlands). The surface images were composed of 1024 × 884 pixels.

The surface fractal dimension, D_s, of AFM and SEM images was calculated by the AP method[26] using the WSxM and ImageJ software programs, respectively. This method proposed by Mandelbrot[27] consists of "sectioning" the surface images with a plane at a given height (e.g., pixel intensity in SEM images). This procedure, equivalent to "filling with water" the structure up to a given level, defines "lake looking" areas (i.e., the water-filled regions) surrounded by higher surface morphology. For the ensemble of lakes so generated, one computes for each lake its corresponding area, A, and perimeter, P. All the data pairs (A,P) are plotted in a double logarithmic graph. These points are arranged along straight line regions with giving a slope M. The values of D_s can then be obtained from the relationship[27,28]

$$D_s = 2M + 1 \quad . \tag{1}$$

For each annealing temperature of a film, a set of five images was analyzed. Each image was "water-filled" at

10 different levels defining "lakes," where the *AP* method was applied following the procedure described in the literature.[23]

III. RESULTS AND DISCUSSION

A. X-ray diffraction analysis

Figure 1 shows the x-ray diffraction (XRD) patterns for platinum films annealed at different temperatures. From as-deposited to samples annealed up to 550 °C, apart from weak diffraction lines originating from the Si substrate, only a broad peak centered around $2\theta = 33°$ was observed. This indicates that the material is amorphous or nanocrystalline. As the annealing temperature was increased to 575 °C, two peaks appeared with high intensity, centered around 39.8° and 46.6°. They correspond to the Pt<111> and the Pt<200> diffraction lines, respectively (CAS number: 7440-06-4). The Pt<111> peak exhibits higher intensity compared with the Pt<200> peak, indicating that preferential growth of the films along the <111> direction. No diffraction peaks from other orientation planes were observed after heat treatment. The appearance of the signal corresponding to the Pt phase upon thermal annealing at 575 °C is in good agreement with the findings of previous work,[15] which showed that <200> metal Pt appeared in the range of 559–626 °C during the heating of platinum oxide films in a pure N_2 atmosphere, without the presence of other phases. Also in that study,[15] heating the films in O_2 atmosphere delayed the decomposition up to 650 °C with the intermediate formation of small amounts of Pt_3O_4. The initial morphology and initial bonding state (related to the *x*-value in PtO_x) may also have a strong impact on the decomposition dynamics. In addition, other authors synthesized directly the Pt phase when reducing the oxygen content to around 25% in the oxygen/argon gas flow during the deposition.[15,29]

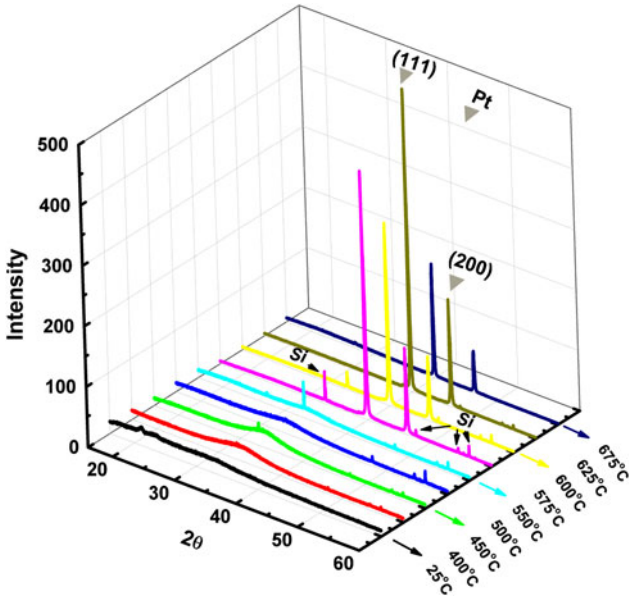

FIG. 1. X-ray diffraction pattern of PtO_x films annealed at different temperatures.

B. Chemical bonding and electronic structure

To investigate the evolution of the chemical states of platinum upon thermal decomposition, the surface composition of the films was studied by XPS. The peak shift caused by the sample charging was corrected by taking into account the shift in the position of the C 1s peak registered without charging at 284.6 eV. The XPS peaks were deconvoluted to determine the peak areas and the binding energies belonging to the different bonding states of platinum. These energies are reported in Table I. They are in good agreement with those reported in the literature.[30,31]

Figure 2 shows the Pt 4f spectra of the as-deposited film and for the films annealed at different temperatures. As can be observed in this figure, several superficial compounds were identified with XPS that could not be identified with XRD. The Pt $4f_{7/2}$ and Pt $4f_{5/2}$ of the as-deposited film showed that the film is mainly composed of PtO_2 and PtO with a composition of 57 and 43 mol%, respectively. For the samples annealed at 400 °C and higher temperature,

TABLE I. X-ray photoelectron spectroscopy data for the different thermal treatment of the PtO_x films.

	Binding energy (eV)									
	Pt		PtO		PtO_2		Percentage of total			
	$4f_{7/2}$	$4f_{5/2}$	$4f_{7/2}$	$4f_{5/2}$	$4f_{7/2}$	$4f_{5/2}$	Pt	PtO	PtO_2	O/Pt ratio
25 °C			71.7	75.1	73.6	76.9		43.0	57.0	1.6
400 °C	71.5	74.9	72.1	75.5	73.6	76.9	10.1	48.9	39.6	1.3
450 °C	71.5	74.9	72.3	75.6	73.9	77.3	12.1	54.8	31.3	1.2
500 °C	71.5	74.9	72.2	75.6	73.8	77.1	30.6	43.7	24.1	0.9
550 °C	71.5	74.9	72.4	75.7	73.8	77.1	43.8	37.8	17.8	0.7
575 °C	70.7	74.0	71.9	75.3	73.8	77.2	70.5	21.3	7.2	0.5
600 °C	70.4	73.7	71.6	75.0	73.7	76.8	71.1	19.2	7.5	0.4
675 °C	69.5	72.9	71.0	74.2	72.3	75.1	76.8	11.8	7.8	0.3

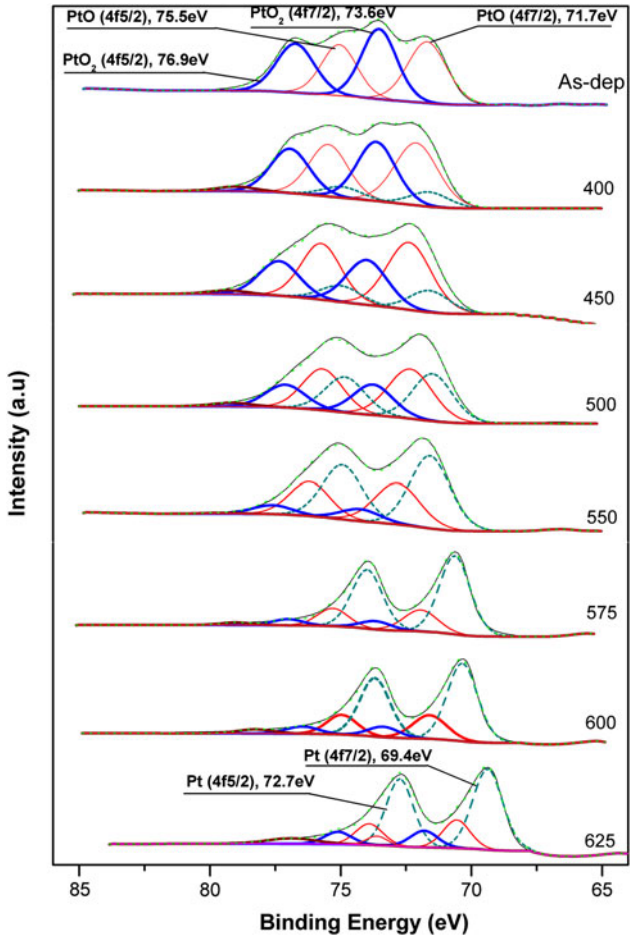

FIG. 2. X-ray photoelectron spectroscopy spectra of PtO_x thin films after annealing at different temperatures (°C) indicated in the curves.

additional contributions appeared at 71.5 and 74.9 eV, both corresponding to Pt. A low-intensity peak at 79 eV can be attributed to plasmon losses. The contribution of this plasmon peak was less than 2% for all the temperatures. As the annealing temperature was further increased from 400 to 550 °C, the peak intensities of both forms of platinum oxide, PtO_2 and PtO, decreased, while the peaks associated to metallic Pt increased. At 575 °C, the intensity of the Pt $4f_{7/2}$ (70.7 eV) and Pt $4f_{5/2}$ (74.0 eV) peaks ascribed to metallic Pt were higher than those of the oxides present indicating that 70.5 mol% of the total composition are now metallic Pt. These observations demonstrate that the decomposition of the oxide surface already started at 400 °C. The O/Pt atomic ratio is reported in Table I and quantifies this decomposition. Some Pt–O bonds can still be detected after annealing at 625 °C; some of which could be ascribed to the bonding of platinum to the silicon surface oxidized upon the thermal annealing in air. Moreover, all contributions present a shift in the binding energy upon annealing. This could originate from slight changes in the phases' stoichiometry.

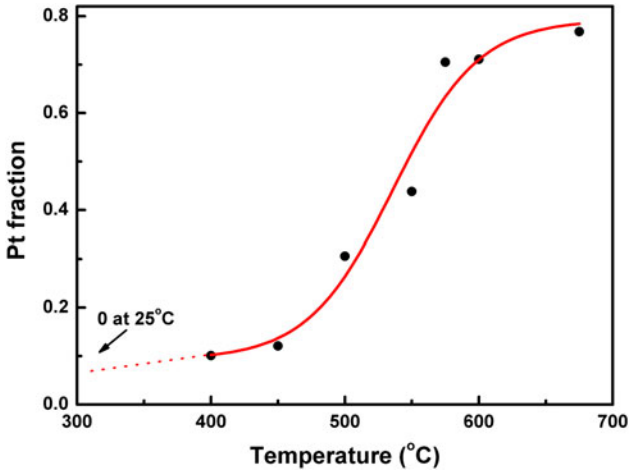

FIG. 3. Platinum fraction in the remaining material following annealing of the original PtO_x films.

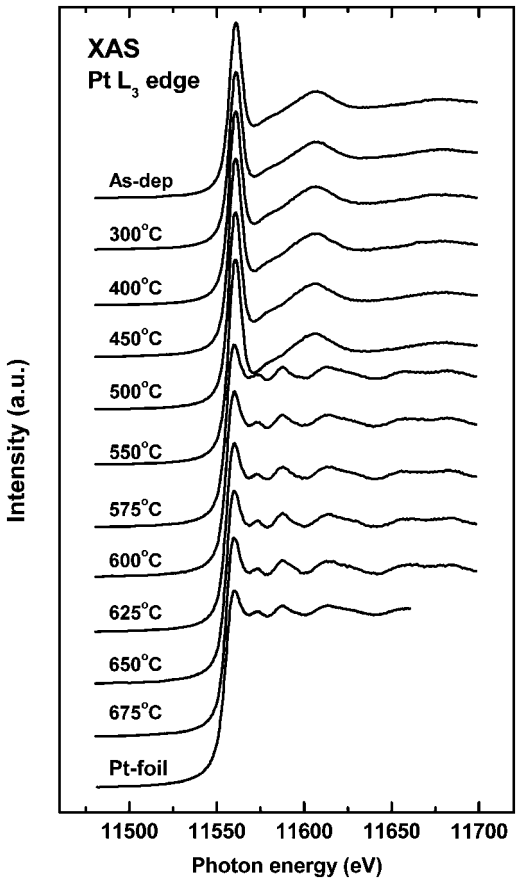

FIG. 4. Pt-L_3 XAS spectra recorded after heat treatment of the PtO_x samples at temperatures indicated on the curves.

Figure 3 shows the molecular fraction of platinum formed during the decomposition process as measured by XPS. The data follow a sigmoid trend. The decomposition rate was slow below 400 °C and accelerated in the 400–575 °C temperature range. These two stages are in line with the findings of Saenger et al.[15] who observed

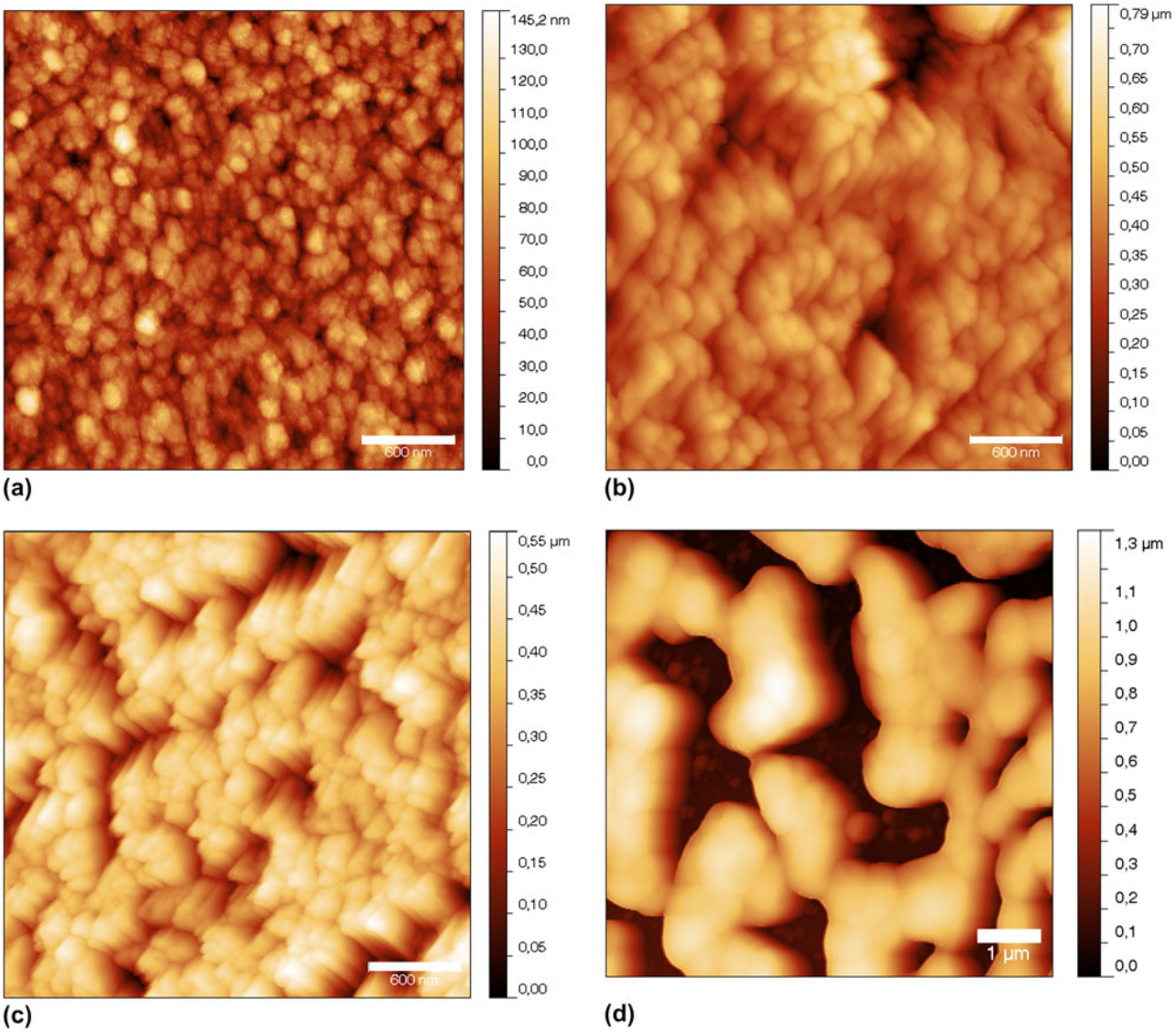

FIG. 5. Atomic force microscopy (AFM) images of PtO_x thin films annealed at different temperatures: (a) 25 °C, (b) 575 °C, (c) 600 °C, and (d) 675 °C.

with XRD a first decomposition stage, with an activation energy of 71 kcal/mol dominating below 400 °C, and a second stage with a lower activation energy of only 25 kcal/mol dominating above this temperature. We additionally observe a third stage above 575 °C for which the process slows down significantly.

Figure 4 shows the X-ray Absorption Spectra (XAS) at the Pt-L_3 absorption edge of PtO_x films deposited on a silicon substrate and subsequently annealed at different temperatures. The top spectrum, labeled "As-dep," corresponds to a PtO_x film without any thermal treatment. The bottom spectrum corresponds to a Pt-foil used as a reference. The first peak after the absorption threshold, at 11550 eV, can be assigned to electronic transitions from the 2p core level to the 5d empty states just above the Fermi energy. It is commonly called the "white line." The intensity of the white line is a measure of the density of empty 5d states. The spectrum of the as-deposited film has the typical lineshape of PtO_2.[32,33] The intensity of the white line in PtO_2 is higher than in metallic Pt because there is a transfer of four 5d electrons from platinum to oxygen, leaving a higher density of 5d empty states in Pt. The region above the white line is governed by multiple scattering processes and, therefore, it is very sensitive to the chemistry and symmetry of the corresponding compounds.

According to Fig. 4, the electronic structure of the films is dominated by the character of oxidized platinum up to a temperature of 550 °C. However, upon annealing between 550 and 575 °C, the XANES of the oxide film approaches that of the Pt foil, which highlights the predominance of metallic Pt in the coatings. Annealing

at higher temperatures does not reveal any further significant structural and chemical evolution of the material. The dynamics of the decomposition of PtO_x thin films can be followed by XPS and XANES providing a much deeper understanding than that gained by XRD. Aside from the evolution of the relative amounts of PtO_2, PtO, and Pt phases, the decomposition process naturally releases oxygen species according to the following reactions:

$$PtO_2 \Rightarrow Pt + O_2 \quad , \tag{2}$$

$$PtO \Rightarrow Pt + {}^1/_2O_2 \quad . \tag{3}$$

It leads to the evolution of the mean molecular volume of the coating. Moreover, the annealing activates atomic diffusion. Hence, the film morphology is expected to undergo significant modifications during decomposition.

C. Fractal properties

AFM images of PtO_x thin films after annealing at different temperatures are shown in Fig. 5. As can be seen, the grains tend to agglomerate at high temperature. This is confirmed by SEM observations (Fig. 6). The topped-dome surface topology as measured by AFM of the samples annealed at 575 and 600 °C [Figs. 5(b) and 5(c)] suggests columnar texture, which is not observed by SEM. Therefore, this topology could be due to a combination of the tip shape and surface of the film as recorded by the AFM tip when the actual microstructure of the film is sharper than the AFM tip, resulting in an image distorted by tip artifacts[34,35] with strong tip convolution effects. This effect is more evident at the imaged slopes of the granular structures.

The SEM images [Figs. 6(b) and 6(c)] reveal a porous morphology due to the decomposition of the platinum oxide phases (PtO_2 and PtO) and reduction of the average molecular volume of the films as stated above.

Figure 7 displays the perimeter as a function of the area of the surface features for all the samples measured by SEM and AFM. The calculated values of the surface fractal dimension D_s of PtO_x thin films annealed at different temperatures are shown in Table II. In general, we can distinguish two regions, each with a characteristic fractal dimension D_{s1} and D_{s2}. This change of regime (slope) takes place at a given crossover area value.

The average roughness *Ra* values shown in Table II were calculated from 3 μm × 3 μm AFM pictures. For temperature below 575 °C, the samples roughness tends to be less than 14.9 ± 0.3 nm, and for temperature above 575 °C, sample roughness (*Ra*) increases with annealing temperature until reaching 301 ± 20 nm.

To correctly analyze fractal dimension, we have to consider the above-mentioned tip-induced artifacts on the AFM images of samples annealed at 575 and 600 °C. Below 575 °C, the AFM data are reliable as judged by the agreement between the AFM and SEM D_s values for

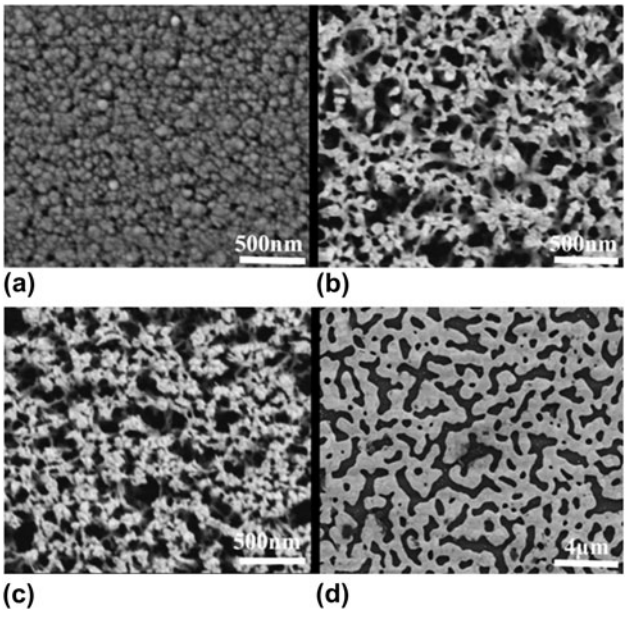

FIG. 6. Scanning electron microscopy (SEM) images of PtO_x thin films annealed at different temperatures: (a) 25 °C, (b) 575 °C, (c) 600 °C, and (d) 675 °C.

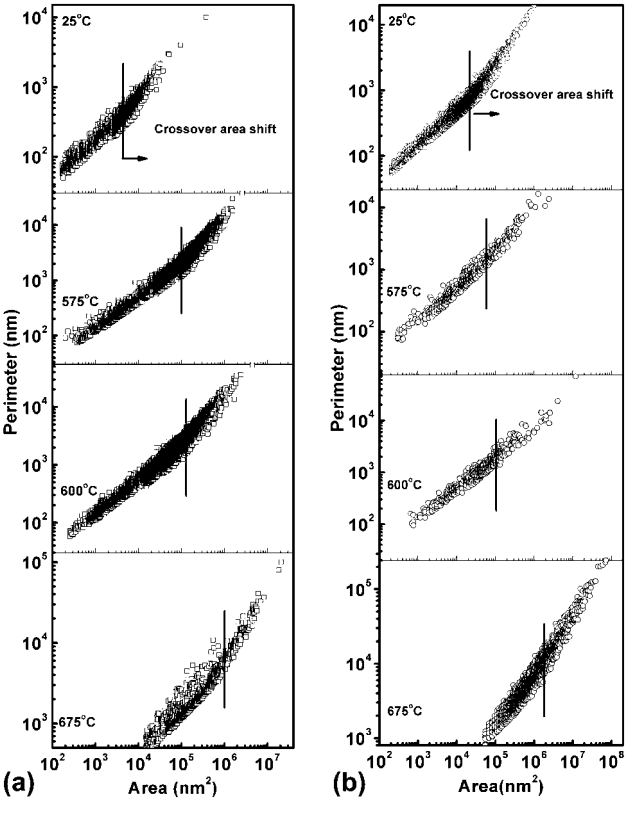

FIG. 7. Perimeter versus area logarithmic plots for samples obtained after annealing at different temperatures and analyzed by (a) SEM and (b) AFM. The change in the slope is the crossover area indicating where the slope changes.

TABLE II. Surface fractal dimension D_s and cross area calculated from the analysis of atomic force microscopy (AFM) and scanning electron microscopy (SEM) images.

Sample temperature (°C)	AFM		SEM		Cross area (nm^2)		Roughness *Ra* (nm)
	D_{s1}	D_{s2}	D_{s1}	D_{s2}	AFM	SEM	AFM
25	2.04 ± 0.14	2.64 ± 0.14	2.04 ± 0.14	2.62 ± 0.14	19630	4202	13.4 ± 0.6
400	2.13 ± 0.14	2.64 ± 0.14	—	—	20026	—	11.1 ± 0.3
550	2.28 ± 0.14	2.87 ± 0.14	—	—	20228	—	14.9 ± 0.3
575	2.16 ± 0.10	2.41 ± 0.10	2.17 ± 0.12	2.79 ± 0.12	53838	104704	74.4 ± 3.5
600	2.09 ± 0.12	2.25 ± 0.12	2.20 ± 0.14	2.69 ± 0.14	67563	120896	68.5 ± 3.1
675	2.29 ± 0.14	2.69 ± 0.14	2.14 ± 0.15	2.86 ± 0.15	1009363	999446	301.0 ± 20.0

the room temperature sample. From 575 °C, it is better to use the data obtained from SEM images as the AFM results can be distorted due to strong tip convolution effects (thus, AFM D_s values tend to be smaller than the SEM-derived values for this temperature range, particularly the D_{s2} values). Once these considerations are taken into account, the fractal dimensions obtained are very similar and only slightly evolve with the annealing temperature. The values of D_{s1} are in the 2.05–2.3 range, i.e., close to 2 indicating that the features exhibiting small area are rather Euclidean without jagged perimeters. In contrast, the values of D_{s2}, which seem to initially increase with the annealing temperature, approach 2.9, which is the percolation limit,[36] indicating highly disordered, fractal surfaces. It is also observed that the crossover area shifts to higher D_s values and the features of smaller area disappear as the annealing temperature is increased. This can be put in relation to the agglomeration of grains that form the film. This decrease in surface area of exchange could be at the origin of the slowing down of the decomposition process above 575 °C. Moreover, as the decomposition starts at the film/air interface, it is possible that oxidized volumes are progressively surrounded by a metallic environment (equivalent of a capping layer) as shown for palladium oxides.[18] Such an environment would limit the oxygen uptake and lower the decomposition rate.

IV. CONCLUSIONS

The thermal decomposition of sputter-deposited platinum oxide PtO_x was studied with different techniques. The as-deposited films were XRD-amorphous or nanocrystalline according to the XRD analysis. Pt 4f XPS investigations indicated that the films were actually composed of PtO_2 and PtO phases. The decomposition started at the surface when the temperature reached 400 °C in ambient air, and it followed a sigmoid trend with further increasing temperature. The evolution of XANES at the Pt-L_3 edge was consistent with the XPS results, but showed that the electronic structure was dominated by oxidized platinum until the temperature reached 575 °C. The AP method applied to SEM and AFM images showed that the film morphology was a combination of large area aggregates and small area granular structures with fractal and Euclidian characteristics, respectively. This analysis also measured the agglomeration of grains in the film with increasing annealing temperature as observed by SEM.

ACKNOWLEDGMENTS

This work was partially supported by the Spanish Ministerio de Educación y Ciencia through project Consolider Ingenio CSD2008-00023 and ENE2010-21198-C04-04. J. Andersson was supported by the Wenner-Gren Foundations and the SSF program MS^2E. We gratefully acknowledge beamtime at the SGM beamline (CLS, Saskatoon) and the KMC-2 beamline (BESSY, Berlin). The research performed at the Canadian Light Source is supported by NSERC, NRC, CIHR, and the University of Saskatchewan. The synchrotron work at BESSY-II was supported by the EC "Research Infrastructure Action" under the FP6 "Structuring the European Research Area Programme" through the "Integrated Infrastructure Initiative Integrating Activity on Synchrotron and Free Electron Laser Science" (Contract no. R II 3-CT-2004-506008). Research at Berkeley Lab was supported by the U.S. Department of Energy under Contract no. DE-AC02-05CH11231.

REFERENCES

1. A. Katayama: Electrooxidation of methanol on a platinum-tin oxide catalyst. *J. Phys. Chem.* **84**(4), 376 (1980).
2. V. Matolín, I. Matolínová, M. Václavu, I. Khalakhan, M. Vorokhta, R. Fiala, I. Pis, Z. Sofer, J. Poltierová-Vejpravová, T. Mori, V. Potin, H. Yoshikawa, S. Ueda, and K. Kobayashi: Platinum-doped CeO_2 thin film catalysts prepared by magnetron sputtering. *Langmuir* **26**(15), 12824 (2010).
3. K. Kuribayashi and S. Kitamura: Preparation of Pt-PtO_x thin films as electrode for memory capacitors. *Thin Solid Films* **400**(1–2), 160 (2001).
4. D. Yamazaki and T. Ueda: Differential platinum thin film hydrogen gas sensor fabricated by MEMS techniques. *IEEJ Trans. Sens. Micromachines* **130**(3), 65 (2010).
5. A. Rajagopal, S. Walavalkar, S. Chen, L. Guo, T. Gwinn, and A. Scherer: Microscaled and nanoscaled platinum sensors. *Appl. Phys. Lett.* **97**(13), 133109 (2010).

6. L. Maya, G.M. Brown, and T. Thundat: Porous platinum electrodes derived from the reduction of sputtered platinum dioxide films. *J. Appl. Electrochem.* **29**(7), 881 (1999).
7. A. Mills: Porous platinum morphologies: Platinised, sponge and black. *Platinum Met. Rev.* **51**(1), 52 (2007).
8. V.E. Dmitrenko, A.A. Trofimova, M.I. Lavrent'ev, G.F. Novikov, and M.B. Artem'eva: Porous platinum electrodes. *Powder Metall. Met. Ceram.* **10**(9), 751 (1972).
9. B. Krishnamurthy and S. Deepalochani: Performance of platinum black and supported platinum catalysts in a direct methanol fuel cell. *Int. J. Electrochem. Sci.* **4**(3), 386 (2009).
10. H.K. Seo, D.J. Park, and J.Y. Park: Fabrication and characterization of platinum black and mesoporous platinum electrodes for in-vivo and continuously monitoring electrochemical sensor applications. *Thin Solid Films* **516**(16), 5227 (2008).
11. Y. Iwai, K. Nakagawa, N. Miura, S. Matsumoto, R. Nakano, and H. Matsumoto: Effect of electrical properties of platinum palladium oxide thin films on the optical properties. *J. Vac. Soc. Jpn.* **52**(3), 163 (2009).
12. H.A. Andreas, S.K.Y. Kung, E.J. McLeod, J.L. Young, and V.I. Birss: Optimization of synthesis parameters employed during Pt nanoparticle formation by in situ reduction. *J. Phys. Chem. C* **111** (36), 13321 (2007).
13. I. Dutta, M.K. Carpenter, M.P. Balogh, J.M. Ziegelbauer, T.E. Moylan, M.H. Atwan, and N.P. Irish: Electrochemical and structural study of a chemically dealloyed PtCu oxygen reduction catalyst. *J. Phys. Chem. C* **114**(39), 16309 (2010).
14. T. Kikuchi, H. Takahashi, and T. Maruko: Fabrication of three-dimensional platinum microstructures with laser irradiation and electrochemical technique. *Electrochim. Acta* **52**(7), 2352 (2007).
15. K.L. Saenger, C. Cabral Jr., C. Lavoie, and S.M. Rossnagel: Thermal stability and oxygen-loss characteristics of Pt(O) films prepared by reactive sputtering. *J. Appl. Phys.* **86**(11), 6084 (1999).
16. L. Maya, L. Riester, T. Thundat, and C.S. Yust: Characterization of sputtered amorphous platinum dioxide films. *J. Appl. Phys.* **84**(11), 6382 (1998).
17. L. Maya, E.W. Hagaman, R.K. Williams, X.D. Wang, G.D. Del Cul, and J.N. Fiedor: Carbon in α-platinum dioxide. *J. Phys. Chem. B* **102**(11), 1951 (1998).
18. D. Horwat, D.I. Zakharov, J.L. Endrino, F. Soldera, A. Anders, S. Migot, R. Karoum, Ph. Vernoux, and J.F. Pierson: Chemistry, phase formation, and catalytic activity of thin palladium-containing oxide films synthesized by plasma-assisted physical vapor deposition. *Surf. Coat. Technol.* **205**(Suppl 2), S171 (2011).
19. G. Lapisardi, L. Urfels, P. Gélin, M. Primet, A. Kaddouri, E. Garbowski, S. Toppi, and E. Tena: Superior catalytic behavior of Pt-doped Pd catalysts in the complete oxidation of methane at low temperature. *Catal. Today* **117**(4), 564 (2006).
20. H. Yamamoto and H. Uchida: Oxidation of methane over Pt and Pd supported on alumina in lean-burn natural-gas engine exhaust. *Catal. Today* **45**(1–4), 147 (1998).
21. G. García-Ayuso, R. Salvarezza, J.M. Martínez-Duart, O. Sánchez, and L. Vázquez: Relationship between the micro structure and the water permeability of transparent gas barrier coatings. *Surf. Coat. Technol.* **100–101**(1–3), 459 (1998).
22. X. Sun, Z. Fu, and Z. Wu: Fractal processing of AFM images of rough ZnO films. *Mater. Charact.* **48**(2–3), 169 (2002).
23. A. Cruz, L. Vázquez, M. Vález, and J. Pérez-Gil, Effect of pulmonary surfactant protein SP-B on the micro- and nanostructure of phospholipid films. *Biophys. J.* **86**(1 Pt I), 308 (2004).
24. B. Mandelbrot: How long is the coast of Britain? Statistical self-similarity and fractional dimension. *Science* **156**(3775), 636 (1967).
25. A.B. Barabási and H.E. Stanley: *Fractal Concepts in Surface Growth*, 1st ed. (Cambridge University Press, New York, 1995).
26. P.D. Sawant and D.V. Nicolau: Nano-topographic evaluation of highly disordered fractal-like structures of immobilized oligonucleotides using AFM. *Mater. Sci. Eng., B* **132**(1–2), 147 (2006).
27. B.B. Mandelbrot, D.E. Passoja, and A.J. Paullay: Fractal character of fracture surfaces of metals. *Nature* **308**(5961), 721 (1984).
28. P. Pfeifer and M. Ober: *The Fractal Approach to Hetereogeneous Chemistry* (Wiley, New York, 1984).
29. J.R. McBride, G.W. Graham, C.R. Peters, and W.H. Weber: Growth and characterization of reactively sputtered thin-film platinum oxides. *J. Appl. Phys.* **69**(3), 1596 (1991).
30. M. Hecq, A. Hecq, J.P. Delrue, and T. Robert: Sputtering deposition, XPS and x-ray diffraction characterization of oxygen-platinum compounds. *J. Less-Common Met.* **64**(2), 25 (1979).
31. Y.C. Chen, Y.M. Sun, S.Y. Yu, C.P. Hsiung, J.Y. Gan, and C.S. Kou: Characterization of Pt oxide thin film fabricated by plasma immersion ion implantation. *Nucl. Instrum. Methods Phys. Res., Sect. B* **237**(1–2), 296 (2005).
32. Y. Nagai, T. Hirabayashi, K. Dohmae, N. Takagi, T. Minami, H. Shinjoh, and S. Matsumoto: Sintering inhibition mechanism of platinum supported on ceria-based oxide and Pt-oxide-support interaction. *J. Catal.* **242**(1), 103 (2006).
33. E.K. Hlil, R. Baudoing-Savois, B. Moraweck, and A.J. Renouprez: X-ray absorption edges in platinum-based alloys. 2. Influence of ordering and of the nature of the second metal. *J. Phys. Chem.* **100** (8), 3102 (1996).
34. K.L. Westra, A.W. Mitchell, and D.J. Thomson: Tip artifacts in atomic force microscope imaging of thin film surfaces. *J. Appl. Phys.* **74**(5), 3608 (1993).
35. P. Grütter, W. Zimmermann-Edling, and D. Brodbeck: Tip artifacts of microfabricated force sensors for atomic force microscopy. *Appl. Phys. Lett.* **60**(22), 2741 (1992).
36. D. Stauffer and A. Aharony: *Introduction to Percolation Theory* (Taylor & Francis, London, 1992).